 CMES, vol.4, no.3&4, pp.421-430, 2003

A Discrete Model for the High Frequency Elastic Wave Examination on Biological Tissue

Jun Liu[1] **and Mauro Ferrari**[1]

Abstract: A microstructure-accounting mechanical field theory approach is applied to the problem of reflection from a granular thin layer embedded between two solid substrates to study the direct relationship of the micro-structural parameters and the overall reflection coefficients of the thin layer. The exact solution for plane wave reflection coefficients is derived under the new theoretical framework giving quantitative relations between the macroscopic reflection coefficients and a set of micro structural/physical parameters including particle size and micromoduli. The model was analyzed using averaged material properties of biological tissue for the granular thin layer. It was demonstrated that changes in micro-level physical and geometrical parameters affect the reflectivity of the thin layer. The results indicate that it is possible to quantitatively determine micro-parameters of the embedded granular material if the reflection spectra are experimentally determined. The effects of micro-parameters also suggest that the discrete representation of biological tissue might be advantageous in modeling its biomechanical responses.

keyword: Biological nanomechanics, granular media, reflection coefficients, thin layer, plane wave propagation.

1 Introduction

The nondestructive determination of material properties of a thin layer embedded between two known materials has generated considerable research interests in recent years [Achenbach, Kitahara, Mikata and Sotiropoulos (1988); Maslov and Kinra (1999); Hwang and Geubelle (2002)]. Both the theoretical modeling and experimental techniques found a wide range of applications in industry and engineering. For example, it is, in many situations, crucial to nondestructively and accurately evaluate the mechanical conditions of an adhesive bond in aerospace engineering [Lanza, Bonomo and Tuzzeo (2001)]. With knowledge about the elastic moduli of the adhesive, the existence of defects or interfacial weaknesses, and the cohesive strength of the bond, decisions can be made whether to further utilize the existing structure or not.

Ultrasonic techniques for the nondestructive evaluation of a thin layer embedded between two substrates usually employ the propagation of elastic waves and evaluate the generated reflection or transmission phenomena at each interface, as well as the multi-reflection/transmission within a thin layer. The theoretical analysis on waves in layered media has been firmly established [Brekhovskikh (1960)]. Experimentally determined reflection coefficients from the thin layer and the dependence of the reflectivity on layer mechanical properties were investigated by [Kinra and Iyer (1995), Lavrentyev and Rokhlin (1997)].

Since the embedded layer could be very "thin", to the extent that the dimension of the microstructures (such as the particle diameter for granular media) is comparable to that of the layer (its thickness), it is here postulated that certain microscopic properties have a macroscopic effect on the overall reflectivity. To our best knowledge, there is little effort devoted to investigating the direct relationship of the microstructures of the layer material and the macroscopic mechanical properties of the layer, and thus the reflectivity, if examined by ultrasonic techniques. Lack of sufficient and convenient theoretical tools may have hindered the research endeavor to address this issue adequately. This paper aims at helping to address this question.

Biological tissue is usually granular or cellular by nature. The onset of disease often causes changes in tissue microstructures. To study these changes and their quantitative correlation with disease, the above described ultrasonic technique may prove useful, because the method could be applied to very small samples, and the application of high frequency elastic waves may lend the mi-

[1] The Ohio State University, Columbus, OH, U.S.A.

crostructures non-negligible. Motivated by these considerations, the theoretical framework of Doublet Mechanics or Nanomechanics [Ferrari, Granik, Imam, and Nadeau, (1997)] is hereby employed to model the plane wave reflection from a granular thin layer and to examine the relationship between the microscopic parameters and the macro-level measurable reflections.

In the field theory of Doublet Mechanics (or Nanomechanics), solids are represented as arrays of points or nodes at finite distances, thus essentially introducing a discrete type of representation of matter. Added to its microstructure-accounting abilities, the distinguishing feature of this theory compared to other micromechanical theories is the fact that it is fully multi-scale, meaning that one can actually navigate from discrete to continuum under the same framework of the theory without resorting to different types of representation. Each lattice node is assumed endowed with a rotation and translation vector with increment vectors that may be expanded in a convergent Taylor series about the lattice nodal point. The order M at which the series is truncated defines the degree of approximation employed. The fundamental equations relating microstrains to the displacement vectors contain the lattice geometry and internodal distances or particle dimensions. The fundamental governing equations of the theory are presented in the Appendix.

The primary interest of this paper is to derive the exact solution for the reflection coefficients of a granular thin layer embedded between two substrates, and to investigate the effect of the microstructural parameters on the reflection coefficients. The overall project aim is to explore the feasibility of ultrasonic interrogation on micro-level characteristics of biological material by using a thin sample. The derivation of the reflection coefficients with plane wave incidence is presented in section 2. With the model obtained from the theoretical derivation, the magnitude of reflection coefficients versus frequency under different parametric settings is plotted and analyzed in section 3. The potential biomedical application of this approach is then discussed in section 4.

2 Derivation of Exact Reflection Coefficients

Consider a configuration where an elastic, discrete-structured (granular) layer of thickness d, is embedded between two infinite, isotropic, elastic domains with perfect bonding (Figure 1). For the purpose of characterizing the mechanical properties of the thin layer with respect to its microstructural features, the discrete-structured layer is identified by its density ρ, the micro elastic constants $A_{\alpha\beta}$, and internodal distances (or particle diameter) η_α. For the definition of the microstructural parameters $A_{\alpha\beta}$ and η_α, reference may be made to the Appendix. The substrates are modeled with continuum elasticity, and the corresponding material properties are density ρ, and Lame's constants: λ and μ.

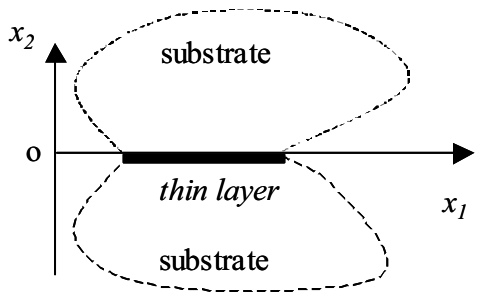

Figure 1 : Schematic of a thin, discrete-structured (granular) layer embedded between two substrates modeled as isotropic elastic continua

A time-harmonic plane wave (longitudinal or shear) is launched at an angle θ from the upper substrate to the structure. The incident wave portions into reflections and transmissions when it hits the first material discontinuity—the upper interface between the thin layer and the substrate. The transmitted waves will further encounter the upper and lower interfaces and cause formation of a series of longitudinal and shear waves propagating up and down within the thin layer. Figure 2 summarizes the types of waves propagating in the system.

As shown in Figure 2, the reflected and transmitted waves propagate as longitudinal or shear waves with different angles and velocities. The angles of the reflection and transmission are dictated by Snell's law, which states that the ratio of the wave number and the sine of the propagation angle remains constant at the same interface. Therefore, there is only one possible angle for each type of waves (longitudinal or shear) propagating in one direction (up or down).

If the displacement vector of the incident wave is known (*i.e.,* the amplitude and the incident angle are known), the other eight waves in the system can be uniquely determined assuming the material properties of the substrates

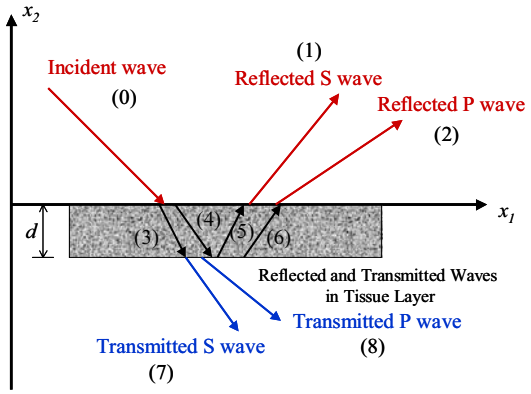

Figure 2 : The nine type of waves propagating in the three-layer structure.

and the layer are known. The displacement of the waves is typically represented in the form of harmonic functions as shown in Equation (1).

$$\mathbf{u}^{(\mathbf{0})} = \mathbf{A_0} \exp\left(ik_0\left(x_1 \sin\theta_0 - x_2 \cos\theta_0 - c_0 t\right)\right) \tag{1}$$

where $\mathbf{u}^{(\mathbf{0})}$ is the displacement of the wave (0), $\mathbf{A}_0$ is the amplitude of the displacement, k_0 is the wave number, θ_0 is the propagation angle with respect to the perpendicular direction, and c_0 is the wave speed.

We define the reflection coefficient for the layer as the magnitude of the ratio of the displacement of the reflected wave from the layer (wave (1) or (2)) over that of the incident wave (Equations (2) and (3)).

$$R_L = \left|\frac{\mathbf{A}_2}{\mathbf{A_0}}\right| \tag{2}$$

$$R_S = \left|\frac{\mathbf{A}_1}{\mathbf{A_0}}\right| \tag{3}$$

where R_L is the reflection coefficient of the reflected longitudinal wave, and R_S is the reflection coefficient of the reflected shear wave. If the incident wave is pulsed, *i.e.*, contains a range of frequency components, the reflection coefficients correspond to that range of frequency generate a reflection spectrum.

In the theoretical framework we employ, the governing constitutive and kinematical equations are multi-scale in nature, with the order of the scale variable in accordance with the problem at study. The objective of this paper is to characterize non-continuum response features that may be of significance in the development of a discrete model for biological tissue. This objective may be reached by limiting our considerations to the approximation degree $M = 2$. For the above-stated plane wave propagation problem, a simplified version of the governing equations is derived with the following assumption: the particle interactions are assumed to be longitudinal (central), so that the shear and torsional microstresses vanish everywhere.

The micro-constitutive relationship corresponding to this assumption is:

$$p_\alpha = \sum_\beta A_{\alpha\beta}\varepsilon_\beta \tag{4}$$

where p_α is the overall microstress in the α *doublet*, and ε_β is the axial microstrain associated with β doublet, $A_{\alpha\beta}$ is the micro elastic constant.

For $M = 2$, the micro-level kinematical relationship is:

$$\varepsilon_\alpha = \tau_{\alpha i}\tau_{\alpha j}\frac{\partial u_i}{\partial x_j} + \frac{1}{2}\eta_\alpha \tau_{\alpha i}\tau_{\alpha j}\tau_{\alpha k}\frac{\partial^2 u_i}{\partial x_j \partial x_k} \tag{5}$$

where ε_α is the micro-strain associated with node α, τ's are

the direction cosines of the unit vectors connecting two nodes, u_i is the displacement in the x_i direction, and η_α is the internal distance associated with node α (assuming all doublets within each bundle share the same internodal distance). For its expanded form please see the Appendix.

The transition from micro to continuum stresses is achieved through imposing natural boundary conditions. The resulting equation follows:

$$\sigma_{ij} = \sum_{\alpha=1}^{n}\left(\tau_{\alpha i}\tau_{\alpha j}p_\alpha - \frac{\eta_\alpha}{2}\tau_{\alpha i}\tau_{\alpha j}\tau_{\alpha k}\frac{\partial p_\alpha}{\partial x_k}\right) \tag{6}$$

where $\sigma_{ij}$is the continuum stress.

The continuum stresses are therefore directly derived from micro level physical and geometrical parameters

such as $A_{\alpha\beta}$, τ's and η_α. Thus, the macro level observable/measurables such as the reflection coefficients from the thin layer are directly related to micro level parameters.

The reflection coefficients may be solved for by enforcing the following continuity conditions at $x_2 = 0$(Equations (7)-(10)) and $x_2 = d$(Equations (11)-(14)):

1. Continuity of normal displacement at $x_2 = 0$:

$$u_1^{(0)} + u_1^{(1)} + u_1^{(2)} = u_1^{(3)} + u_1^{(4)} + u_1^{(5)} + u_1^{(6)} \tag{7}$$

2. Continuity of normal stress at $x_2 = 0$:

$$\sigma_{22}^{(0)} + \sigma_{22}^{(1)} + \sigma_{22}^{(2)} = \sigma_{22}^{(3)} + \sigma_{22}^{(4)} + \sigma_{22}^{(5)} + \sigma_{22}^{(6)} \tag{8}$$

3. Continuity of shear displacement at $x_2 = 0$:

$$u_2^{(0)} + u_2^{(1)} + u_2^{(2)} = u_2^{(3)} + u_2^{(4)} + u_2^{(5)} + u_2^{(6)} \tag{9}$$

4. Continuity of shear stress at $x_2 = 0$:

$$\sigma_{21}^{(0)} + \sigma_{21}^{(1)} + \sigma_{21}^{(2)} = \sigma_{21}^{(3)} + \sigma_{21}^{(4)} + \sigma_{21}^{(5)} + \sigma_{21}^{(6)} \tag{10}$$

5. Continuity of normal displacement at $x_2 = -d$:

$$u_1^{(7)} + u_1^{(8)} = u_1^{(2)} + u_1^{(4)} + u_1^{(5)} + u_1^{(6)} \tag{11}$$

6. Continuity of normal stress at$x_2 = -d$:

$$\sigma_{22}^{(7)} + \sigma_{22}^{(8)} = \sigma_{22}^{(3)} + \sigma_{22}^{(4)} + \sigma_{22}^{(5)} + \sigma_{22}^{(6)} \tag{12}$$

7. Continuity of shear displacement at$x_2 = -d$:

$$u_2^{(7)} + u_2^{(8)} = u_2^{(3)} + u_2^{(4)} + u_2^{(5)} + u_2^{(6)} \tag{13}$$

8. Continuity of shear stress at$x_2 = -d$:

$$\sigma_{21}^{(7)} + \sigma_{21}^{(8)} = \sigma_{21}^{(3)} + \sigma_{21}^{(4)} + \sigma_{21}^{(5)} + \sigma_{21}^{(6)} \tag{14}$$

where $\sigma_{ij}^{(n)}$ is the stress associated with the nth wave (the waves are numbered from 0 to 8 as shown in Figure 2; and $u_m^{(n)}$ is the displacement associated with the nth wave.

The above boundary conditions give an 8X8 matrix by which the reflection coefficients (R_L or R_S) can be solved for assuming the incident wave and the material properties of the substrate and the thin layer are known.

3 An application of the theory: microstructure-accounting analysis of biological tissue samples

The theoretical model described above is applied in this section to analyze thin biological tissue samples on microscopic slides. In medical histology laboratories, biological tissue specimens are typically sectioned and placed between two glass slides. In this section it will be shown how the above-developed theory may be employed in the course of high frequency elastic wave (ultrasound) interrogation in order to identify features that correlate with the sample microstructure.

The following setup is adopted for the illustrative simulation:

1. Substrates: crown glass [Weast (1985)]:
   Density=2.5 g/cm^3
   Lame's constants are:
   λ = 26.4 GPa
   μ = 29.0 GPa.

2. Thin layer: soft tissue

Soft tissue is chosen to be the material of the thin layer. For the forward problem, the properties of the thin layer are assumed known too.

To obtain numerical solutions for the Nanomechanics modeling problem, we focus our attention on the microstructure shown in Figure 3. This arrangement results in 3D macroscopic isotropy [Ferrari, (2000)] if the order of the scale is chosen to be one ($M = 1$). It also reduces the number of the independent micromoduli to two: A_{11} and A_{44}.

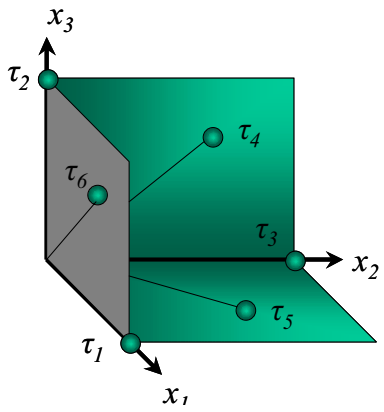

Figure 3 : Micro-architecture of the doublets associated with the node at the origin

The direction cosine matrix is as follows:

$$\begin{array}{ll} \tau_1 = (1,0,0) & \tau_4 = (0,1/\sqrt{2},1/\sqrt{2}) \\ \tau_2 = (0,1,0) & \tau_5 = (1/\sqrt{2},0,1/\sqrt{2}) \\ \tau_3 = (0,0,1) & \tau_6 = (1/\sqrt{2},1/\sqrt{2},0) \end{array} \quad (15)$$

The micromoduli of the tissue are estimated from macro elastic moduli based on the fact that the multi-scale model reduces to the continuum model when the scale factor is equal to one. Specifically, the micromoduli are related to Lame's constants as follows [Ferrari, (2000)]:

$$\begin{array}{l} \lambda = A_{11} - A_{44} \\ \mu = \frac{1}{4} A_{44} \end{array} \quad (16)$$

The values of the macro elastic moduli of the thin tissue layer are adopted from the averaged values for human breast tissue in the literature [Goss, Johnston, and Dunn, (1978), (1980)]. It is also hypothesized that the dimension of the nodes in the discrete model for the biological tissue corresponds to that of the cells. We assume that the cells are close-packed so that the internodal distance is equivalent to the cell diameter. The typical dimension of human breast epithelial cells is 10-μm. We further assume that the internodal distances are the same for all doublets in this simulation. Therefore $\eta_\alpha = \eta$ and is at the scale of 10-μm.

Therefore, we assume the set of parameters for the biological tissue thin layer as follows:

Density: 1.0 g/cm^3

A_{11}=3.0 GPa

A_{44}=0.5 GPa

$\eta = 1 \sim 10 - \mu$m

The thickness of the thin layer is assumed to be 150-μm, which is thin enough to be considered a "thin" layer compared to the dimension of the substrates (glass slides) and thick enough to accommodate several nodes (cells) cross the thickness. The incident angle can be any arbitrary angle if its magnitude is between those of the two mode conversion angles for the glass-tissue interface. Without losing generality, 47 degrees is chosen to be the incident angle for all the simulations in this study.

Computer simulations for generating the reflection coefficients from the thin tissue layer are thus conducted to investigate the following questions:

1. The advantages of the higher order form of the multi-scale Nanomechanics model compared to continuum mechanics model;
2. The effect of microstructural properties on the overall reflection coefficients/spectra of the thin layer under the framework of Nanomechanics.

3.1 Comparison of Nanomechanics and Continuum Mechanics Prediction on the Reflection Coefficients

The simulation results from two scales are compared: $M = 1$(non-scale) and $M = 2$, with all other parameters chosen to be the same and specified as above. For the $M = 1$ case, the exact solution for the reflection coefficients is the same as that modeled from continuum mechanics [Ferrari, Granik, Imam, and Nadeau, (1997)]. For the $M = 2$ case, the reflection coefficients are calculated following the derivation described in section 2.

The first simulation considers a medium with small internodal distance (1-μm) that is examined by fairly low frequency elastic waves (¡15 Mhz). The result is shown in Figure 4. It appears that the prediction from the Nanomechanics and the continuum theory on the reflection coefficients are essentially identical.

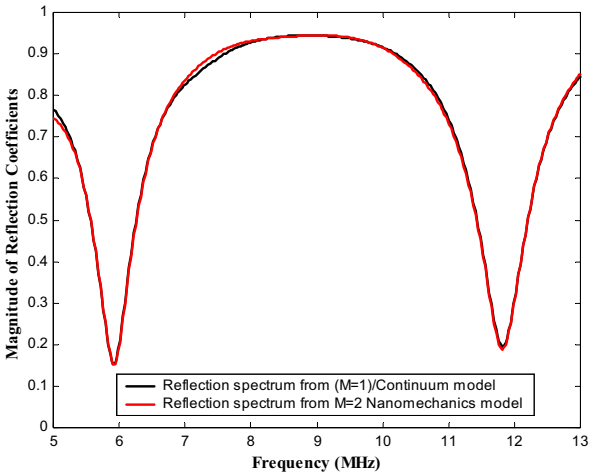

Figure 4 : The reflection spectrum from continuum model (dashed line) and that from nanomechanics model (solid line) for "very small" internodal distance ($\eta = 1 - \mu$m).

The result is not surprising, because for a medium with very small internodal distance, the nodes/particles are "invisible" for low frequency elastic waves whose wavelength is much greater than the dimension of the particles. Under this condition, the predicted response from

the discrete model is known to converge to that from conventional continuum models. Nevertheless, the nanomechanics model offers the opportunity to correlate the response of the medium to its microstructural characteristics. For example, if the size of the particles is varied while other properties remain the same, a change in the reflection coefficient is observed, as shown in the following simulation. Thus, the Nanomechanics model gives insight to the upper limit of the size of the particles before they become "visible" for elastic waves propagating at a certain range of frequencies.

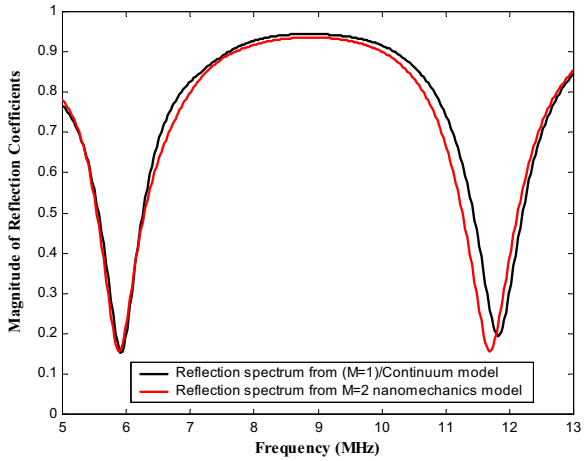

Figure 5 : The reflection specturm from continuum model (dashed line) and that from nanomechanics model (solid line) for "larger" internodal distances ($\eta = 8 - \mu$m).

Figure 5 shows the result of the second simulation where every other parameter remains the same except the internodal distance, which is set to be 8-μm. The resulting reflection spectrum shows appreciable difference compared to that generated from continuum model. The particle size (or internodal distance) in this case is still far below the magnitude of the wavelength (20$\sim$350-μm).

If the internodal distance remains the same (1-μm), and the frequency of the elastic waves is much higher (¿ 50Mhz), substantial discrepancy in the prediction of the reflection spectra from the two models is also observed (Figure 6).

3.2 The Effect of Micromoduli

With all the other parameters fixed, the micromodulus A_{11} is varied $\pm$10% to study its effect on the reflection

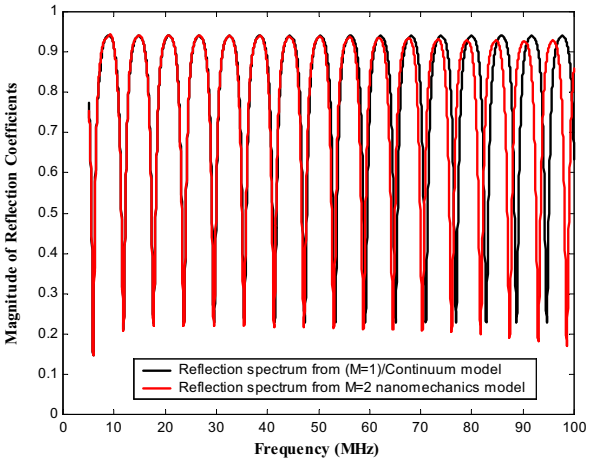

Figure 6 : The comparison between nanomechanics model and continuum model at lower and higher frequencies for "very small" internodal distance ($\eta = 1 - \mu$m).

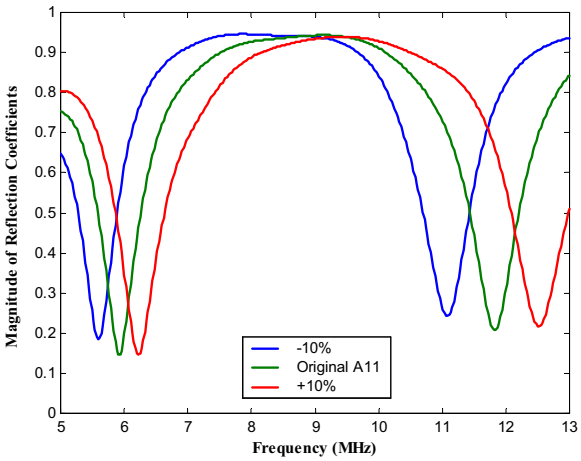

Figure 7 : The effect of the A_{11}

spectrum.

Figure 7 shows that increase in micromodulus A_{11} results in shifting of the overall spectrum to the right (higher frequency), and vice versa. The changes in micromodulus A_{11} change the location of the minima in the curves. Nevertheless, the magnitude of the minima and the distance between the minima remain unaffected.

Similarly the effect of modulus A_{44} is studied by varying its magnitude to $\pm$10% of the original. The result is shown in Figure 8.

Figure 8 shows that A_{44} affects the overall reflection spectra to a much lesser degree compared to A_{11}. In other

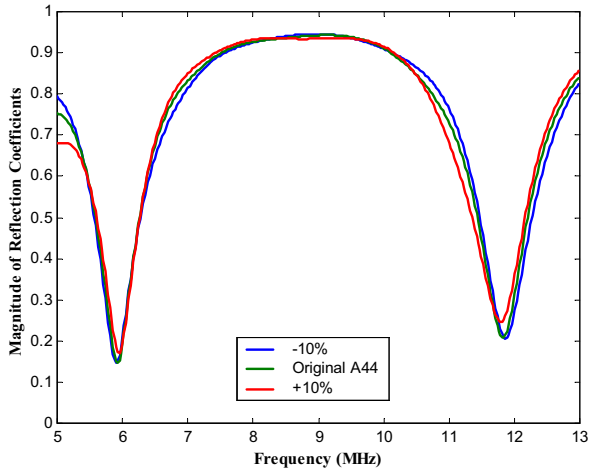

Figure 8 : The effect of A_{44} with 10% variation

words, A_{44} is a less sensitive parameter in terms of determining the reflection spectrum. To study its general effect, a greater amount of change (20%) is introduced and the result is shown in Figure 9.

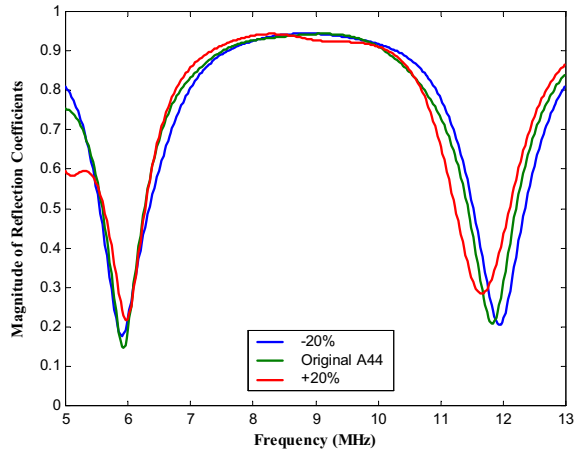

Figure 9 : The effect of A_{44} with 20% variation

Figure 9 shows that increase in micromodulus A_{44} results in shifting of the second minimum to the left (lower frequency), and vice versa. Therefore changes in micromodulus A_{44} change the distance between the two minima, and also the magnitude of the minima.

3.3 Effect of Particle Size (Internodal Distance/Cell Size)

With all the other parameters fixed, the particle size of the thin layer is varied $\pm 20\%$ to study its effect on the reflection spectrum (Figure 10).

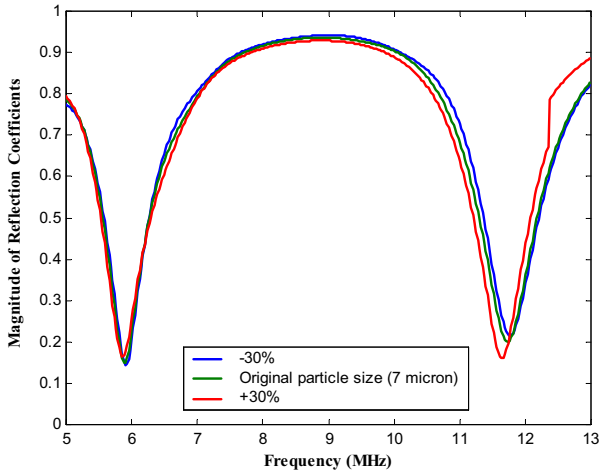

Figure 10 : The effect of particle size at lower frequencies.

Figure 10 shows that the particle size has minimal effect on the overall reflection spectrum at the relatively low frequency range. For higher frequency range, the simulation result is shown in Figure 11.

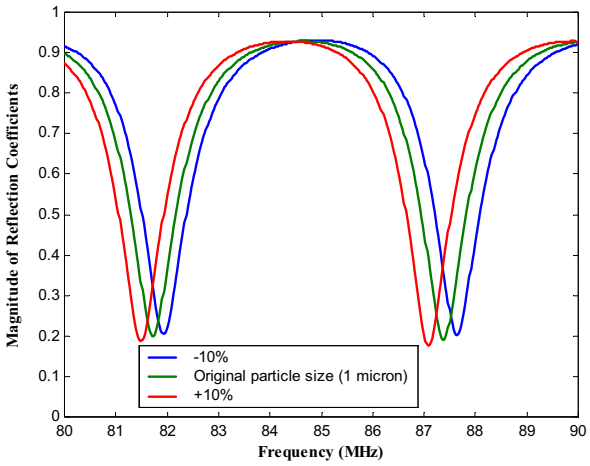

Figure 11 : The effect of particle size at higher frequencies.

It appears that at higher frequency range the particle size has an appreciable effect on the reflection spectrum by

shifting it to the left with increased magnitude of the particle size. This effect is similar to that of micromodulus A_{11}, however, the effects of the two parameters differ: changes in micromodulus A_{11}has the same effect on the reflection spectra regardless of the frequency range, while the effect of particle size is frequency dependent.

4 Discussion and Conclusion

In this paper, the forward problem was solved, *i.e.*, the exact solution for the reflection coefficients of a thin layer embedded between two substrates. The reflectivity of the thin layer was shown to be affected by the micro-level parameters of the granular layer, including micromoduli and particle size. The simulation was studied utilizing a configuration that is routine to pathological settings: a histology slide where a very thin tissue section is embedded between two glass slides.

The inverse version of this problem, by which the parameters of the thin layer are unknown, but the reflection coefficients are measured experimentally, is of particular interest for pathological applications. Histology slides are examined by pathologists under a microscope to analyze microstructural features that contain diagnostic information. It is the relationship between the cellular structures—the micro architecture that affords useful diagnostic criteria to separate normal tissue from malignancies, and further different types of malignancies. Pathologists may read microstructures under the microscope; however, even microstructure information sometimes is not sufficient. For example, well-differentiated malignant tissue has very similar cell distribution patterns compared to normal tissue [Cotran, Kumar and Collins (1999)]. Pathologists resort to macro-level examination on physical properties of the tissue, such as X-ray or ultrasound imaging, or molecular analysis from immunostaining for additional diagnostic information to be integrated into that from histology slide analysis.

If inversion algorithms are developed to reconstruct tissue properties from experimental data and the theoretical model, the backward/inverse problem can be solved for. This presents a potential to design an automatic pathology slide reader that "reads" histology slides and interprets the reflection spectra for separating malignant and normal tissue based on information of the tissue properties, including mechanical properties (micromoduli) and microstructural features (particle size).

We have designed an apparatus to measure the reflection spectra from tissue samples prepared as a sandwich structure with a thin slice of tissue being placed between two pieces of glass slides. For detailed information on the experimental setup, reference is made to [Liu, Rokhlin and Ferrari, (2002)]. Typical reflection spectra from normal and malignant breast tissue are shown in Figure 12.

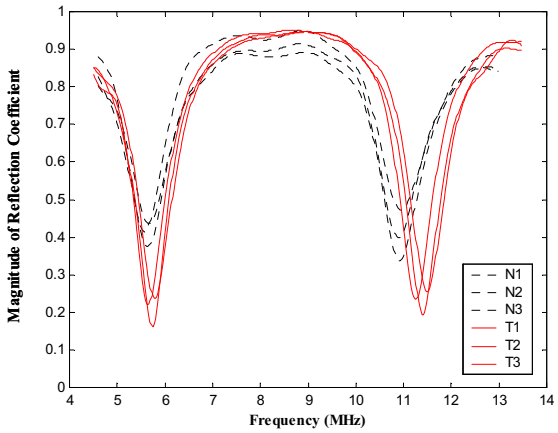

Figure 12 : Comparison of experimentally measured reflection spectra from normal breast tissue and malignant breast tissue (invasive ductal carcinoma). N1, N2, and N3 are the reflection spectra from three normal tissue sections; T1, T2 and T3 are those from three malignant tissue sections.

It appears that the reflection spectra of the normal and malignant breast tissue differ in several aspects: the locations of the minima, the distance between the minima, and the magnitude of the minima. According to the theoretical analysis of the effects of the tissue properties on the overall reflection spectrum presented in section three, these differences could be accounted for by the microstructural mechanisms such as the difference in micromoduli or the internodal distances.

In conclusion, this study presents a novel approach for the constitutive modeling and thus characterization of the mechanical properties of biological tissue in accordance to its microstructures.

Acknowledgement: The authors wish to thank Dr. Stanislav Rokhlin and his associates for providing ultrasonic experimental instruments and helpful discussions on the model derivation. We are also grateful for Mrs. Mary Marin and Mrs. Karen Williams for preparing the

tissue samples, and Mr. Shawn Coontz for providing the glass slides used for obtaining the experimental results in this study.

References

Achenbach J.D.; Kitahara M.; Mikata Y.; Sotiropoulos D.A. (1988): Reflection and transmission of plane-waves by a layer of compact inhomogeneities, Pure And Applied Geophysics, 128: (1-2) 101-118

Brekhovskikh, L., (1960): *Waves in Layered Media*, Academic Press Inc. (London) Ltd.

Cotran R. S.; Kumar V.; Collins T. (1999): *Robbins Pathological Basis of Disease*, W.B. Saunders Company

Ferrari, M. (2000): Nanomechanics, and Biomedical Nanomechanics: Eshelby's Inclusion and Inhomogeneity Problems at the Discrete/Continuum Interface, *Biomedical Microdevices*, 2(4): 272-281

Ferrari, M.; Granik, V.T.; Imam, A.; Nadeau, J., (1997): *Advances in Doublet Mechanics*, Springer

Goss, S. A.; Johnston, R. L.; and Dunn, F., (1978): Comprehensive compilation of empirical ultrasonic properties of mammalian tissues, I, *Journal of the Acoustical Society of the America*, 64, 423-457

Goss, S. A.; Johnston, R. L.; and Dunn, F., (1980): Comprehensive compilation of empirical ultrasonic properties of mammalian tissues, II, *Journal of the Acoustical Society of the America*, 68, 93-108

Granik, V. T.; Ferrari, M., (1993): Microstructural mechanics of granular media, *Mechanics of Materials*, 15,301-322

Hwang, C.; Geubelle, P. H., (2000): A spectral scheme to simulate dynamic fracture problems in composites, *CMES: Computer Modeling in Engineering & Sciences*, 1(4): 45-55, 2000

Kinra, V.K.; Iyer, V.R. (1995): Ultrasonic measurement of the thickness, phase velocity, density or attenuation of a thin-viscoelastic plate. Part II: the inverse problem. *Ultrasonics*, 33(2): 111-122

Liu, J.; Rokhlin S.I., Ferrari, M. (2003): Ultrasonic determination of the mechanical properties of thin biological tissue sections, *Manuscript in preparation*

Lanza S.F.; Bonomo, M.; Tuzzeo, D. (2001): Ultrasonic guided wave inspection of bonded lap joints: Non-contact method and photoelastic visualization, *Research in Nondestructive Evaluation* 13(3): 153-171

Lavrentyev, A. I.; Rokhlin, S. I., (1997): Determination of elastic moduli, density, attenuation, and thickness of a layer using ultrasonic spectroscopy at two angles, *Journal of the Acoustical Society of the America*, 102(6), 3467-3477

Maslov K.; Kinra V.K. (1999): Acoustic response of a periodic layer of nearly rigid spherical inclusions in an elastic solid, *Journal of the Acoustical Society of the America*, 106: (6) 3081-3088

Weast, R.C. (Editor in chief); **Astle, M.J.; Beyer, W. H.** (Associate editors) (1985-1986): *CRC Handbook of Chemistry and Physics*, CRC Press, Inc.

Appendix

For the ease of visualization, a granular interpretation of the theory is introduced: the solid is modeled as a regular array of equal-sized elastic spheres of diameter d,the centers of which form Bravais lattice. It is noted that the theory itself does not require such an interpretive aid.

The displacements of the particles are assumed to vary little at the lengths on the order of their separations. A smooth vector field of the translation function $\mathbf{u}(\mathbf{X},t)$ is introduced, where $\mathbf{X}$ is the position vector of an arbitrary point in the body and t is time. The vector field of the translation displacement is assumed to coincide with the real translation of the granular body particles at the node a, where $\mathbf{X}=\mathbf{x}$.

An incremental vector Δu_α is introduced, which is defined as

$$\Delta\mathbf{u}_\alpha = \mathbf{u}(\mathbf{x}+\boldsymbol{\zeta}_\alpha,t)-\mathbf{u}(\mathbf{x},t) \tag{A-1}$$

It represents an increment of the translation vector $\boldsymbol{u}$ in a transition from an arbitrary node a to the adjacent node b_α (Figure A-1).

The above increment vector may be expanded in a convergent Taylor series in a neighborhood of an arbitrary node a whose position vector is $\mathbf{x}$. Truncating this series at the $M-$th term we obtain

$$\Delta u_\alpha = \sum_{\chi=1}^{M}\frac{(\eta_\alpha)^\chi}{\chi!}(\tau_\alpha\cdot\nabla)^\chi u(x,t) \tag{A-2}$$

when $X=x$.

Based on the above assumptions, the axial microstrain is

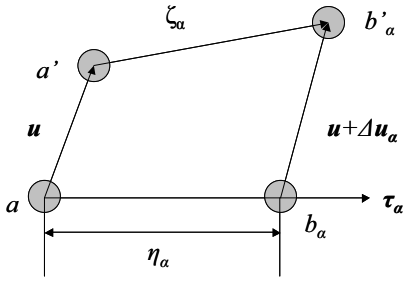

Figure A-1 : Translations of the doublet nodes a and b_α, η_α is the distance between the two doublet nodes, $\boldsymbol{\pi}_\alpha$ is the unit vector along the original direction from node a to b_α, and $\boldsymbol{\zeta}_\alpha$ is the new direction vector after the deformation.

obtained

$$\varepsilon_\alpha = \tau_{\alpha i} \sum_{\chi=1}^{M} \frac{(\eta_\alpha)^{\chi-1}}{\chi!} \tau_{\alpha k_1} \cdots \tau_{\alpha k_\chi} \frac{\partial^\chi u_i}{\partial x_{k_1} \cdots \partial x_{k_\chi}} \tag{A-3}$$

It follows that the first approximation $(M = 1)$ for the axial microstrain takes the form

$$\varepsilon_\alpha = \tau_{\alpha i} \tau_{\alpha j} \varepsilon_{ij} \tag{A-4}$$

where $\varepsilon_{ij} = \frac{1}{2}(\frac{\partial u_i}{\partial x_j} + \frac{\partial u_j}{\partial x_i})$

And the second approximation $(M = 2)$ takes the form

$$\varepsilon_\alpha = \tau_{\alpha i} \tau_{\alpha j} \frac{\partial u_i}{\partial x_j} + \frac{1}{2} \eta_\alpha \tau_{\alpha i} \tau_{\alpha j} \tau_{\alpha k} \frac{\partial^2 u_i}{\partial x_j \partial x_k} \tag{A-5}$$

in expansion, it becomes:

$$\begin{aligned} \varepsilon_\alpha &= \tau_{\alpha 1}^2 \frac{\partial u_1}{\partial x_1} + \tau_{\alpha 1} \tau_{\alpha 2} (\frac{\partial u_1}{\partial x_2} + \frac{\partial u_2}{\partial x_1}) + \tau_{\alpha 2}^2 \frac{\partial u_2}{\partial x_2} \\ &+ \frac{\eta_\alpha}{2} \left(\tau_{\alpha 1}^3 \frac{\partial^2 u_1}{\partial x_1^2} + 2\tau_{\alpha 1}^2 \tau_{\alpha 2} \frac{\partial^2 u_1}{\partial x_1 \partial x_2} + \tau_{\alpha 2}^2 \tau_{\alpha 1} \frac{\partial^2 u_1}{\partial x_2^2} \right. \\ &\left. + \tau_{\alpha 1}^2 \tau_{\alpha 2} \frac{\partial^2 u_2}{\partial x_1^2} + 2\tau_{\alpha 2}^2 \tau_{\alpha 1} \frac{\partial^2 u_2}{\partial x_1 \partial x_2} + \tau_{\alpha 2}^3 \frac{\partial^2 u_2}{\partial x_2^2} \right) \end{aligned} \tag{A-6}$$

Microstress p_α that is associated with ε_α is defined. The microstress-microstrain constitutive relationship is:

$$p_\alpha = \sum_{\beta=1}^{n} A_{\alpha\beta} \varepsilon_\beta \tag{A-7}$$

where $A_{\alpha\beta}$ are the micro-level elastic moduli. This relationship is obtained under the assumption that the particle interactions are longitudinal (central), so that the shear and torsional microstresses vanish everywhere.

The transition from microstresses to macrostresses is achieved by applying equilibrium equations and the resulting relationship is

$$\sigma_{k_1 i}^{(M)} = \sum_{\alpha=1}^{n} \tau_{\alpha k_1} \sum_{\chi=1}^{M} (-1)^{\chi+1} \frac{(\eta_\alpha)^{\chi-1}}{\chi!}$$

$$\tau_{\alpha k_2} \cdots \tau_{\alpha k_\chi} \frac{\partial^{\chi-1}(p_{\alpha i})}{\partial x_{k_2} \cdots \partial x_{k_\chi}} \tag{A-8}$$

(A-9)

The first approximation $(M = 1)$ for the stress takes the form

$$\sigma_{ij} = \sum_{\alpha=1}^{n} \tau_{\alpha j} \tau_{\alpha i} p_\alpha \tag{A-10}$$

It is further derived that the macromoduli for $M = 1$case becomes

$$C_{ijkl} = \sum_{\alpha,\beta=1}^{n} A_{\alpha\beta} \tau_{\alpha i} \tau_{\alpha j} \tau_{\beta k} \tau_{\beta l} \tag{A-11}$$

The second approximation $(M = 2)$ for the continuum stress takes the form

$$\sigma_{ij} = \sum_{\alpha=1}^{n} \tau_{\alpha j} (\tau_{\alpha i} p_\alpha - \frac{1}{2} \eta_\alpha \tau_{\alpha k} \tau_{\alpha k} \frac{\partial p_\alpha}{\partial x_k}) \tag{A-12}$$

The more general variants of the theory are introduced in [Ferrari, Granik, Imam, and Nadeau, (1997)].